Chemical Science

ROYAL SOCIETY OF CHEMISTRY

EDGE ARTICLE

View Article Online
View Journal | View Issue

Cite this: *Chem. Sci.*, 2025, **16**, 14534

All publication charges for this article have been paid for by the Royal Society of Chemistry

Acceleration and regioselectivity switching in 1,3-dipolar cycloaddition reactions confined in a bis-calix[4]pyrrole cage†

Yifan Li, [ab] Gemma Aragay [a] and Pablo Ballester *[ac]

We report the results of our investigations on the role of the octa-imine bis-calix[4]pyrrole cage **1** in mediating confined 1,3-dipolar cycloaddition reactions of a series of 4-azido(alkyl)-pyridine-*N*-oxides (alkyl = null, Me, Et; **2a–c**) with 1-(2-propynyl)-4(1*H*)-pyridinone (**4**). We performed ^{1}H NMR binding studies of the different substrates with the octa-imine cage, evidencing the formation of thermodynamically and kinetically highly stable inclusion homo-complexes featuring 1 : 1 and 2 : 1 stoichiometry. We used simulated speciation profiles and performed ITC experiments to thermodynamically characterize the formed complexes. Adding mixtures of an azido-derivative with the propynyl–pyridinone in a solution of cage **1** resulted in the formation of the expected 1 : 1 and 2 : 1 homo-complexes, and allowed the detection and characterization of the corresponding ternary hetero-complexes (Michaelis) in solution, **2**·**4**⊂**1**. The azide–alkyne cycloaddition reactions are significantly accelerated by confinement of the reactants in cage **1**. We assessed the reactions' acceleration factor by determining their effective molarities (EM = k_{intra}/k_{bulk}). We derived the k_{intra} values from the best-fit computer simulation of an elaborated theoretical kinetic model to the experimental kinetic data. The determined EM values range from 2000 to 70 M depending on the length of the azido(alkyl) spacer. Notably, we observed a complete switching in the regioselectivity of the confined cycloaddition reactions. That is, the confined reaction is stereoselective for the 1,4-isomer of the triazole adduct of the 4-azido pyridine-*N*-oxide derivative **2a**, but turns stereoselective for the 1,5-counterpart for the azido(methyl) and azido(ethyl) derivatives, **2b** and **2c**. We used the computed DFT structures of the inclusion complexes to rationalize our findings.

Received 25th April 2025
Accepted 6th July 2025

DOI: 10.1039/d5sc03033a

rsc.li/chemical-science

Introduction

Chemists have designed and synthesized molecular containers inspired by enzymes,[1,2] and used their cavities as nanometric flasks to mediate intra- and inter-molecular reactions.[3,4] Similarly to enzymes' active sites, the simple inclusion of two reacting substrates within the confined space of a synthetic molecular flask increases their local concentration. Considering identical bulk concentrations, this simple confinement effect can significantly increase the bimolecular reaction rate compared to that in solution. However, confined reactions might experience other effects.[5,6] The confinement process can arrange and orient the reacting groups of the substrates in a geometry close to that of the reaction's transition state (TS). In doing so, the binding of the substrates in the container's cavity can compensate for additional entropic costs of the reaction, thereby further reducing the energy barrier of the TS ($\Delta S^{\ddagger}$).[2]

Enthalpic stabilization of the TS, desolvation, and others have also been postulated to explain the reaction's acceleration induced by confinement.[7,8] Controlling the relative orientation of the reacting groups within the confined reaction space can significantly influence the reaction's selectivity.[9,10] This control is mainly exerted by size, shape, and functional groups complementarity between the substrates and cavities, as well as the minimization of steric clashes. Examples were reported in which the selectivity of the confined reaction was significantly altered[11,12] or even completely changed[13] compared to the bulk.

In short, the simultaneous binding of two reacting substrates in a molecular container leads to the formation of a ternary hetero-complex (*a.k.a.* Michaelis complex). This is a key feature of the confinement effect in bimolecular reactions, which, due to multiple factors, influences the reaction's rate and selectivity.[9,14]

[a]*Institute of Chemical Research of Catalonia (ICIQ), The Barcelona Institute of Science and Technology (BIST), 43007 Tarragona, Spain. E-mail: pballester@iciq.es*

[b]*Departament de Química Analítica i Química Orgànica, Universitat Rovira i Virgili, 43007 Tarragona, Spain*

[c]*ICREA, 08010 Barcelona, Spain*

† Electronic supplementary information (ESI) available: General information and instruments, synthetic procedures, characterization of compounds **4**, **7a–c**, and **8b–c**, binding studies, theoretical kinetic models, kinetic and thermodynamic characterization of cycloaddition reactions. See DOI: https://doi.org/10.1039/d5sc03033a

Designing tailored molecular containers to facilitate specific chemical reactions is a complex task.[15] Typically, these containers are synthetically challenging to access, and their customization involves intricate procedures.[16] Additionally, predicting the influence of a molecular container on the confined chemical reaction (*i.e.*, acceleration and selectivity) is not straightforward.

In the last few decades, the azide–alkyne Huisgen cycloaddition reaction has been widely studied. This 1,3-dipolar cycloaddition reaction grants access to triazole derivatives, which are highly relevant to medicinal chemistry and pharmacology.[17] In the bulk solution, the inter-molecular version of the reaction is typically very slow, even at high temperatures, producing a mixture of two regioisomeric products: 1,4- and 1,5-disubstituted 1,2,3-triazoles.[18] The Cu(I)-catalyzed azide–alkyne cycloaddition (CuAAC) reaction is a well-established and highly efficient procedure for the regioselective synthesis of 1,4-substituted 1,2,3-triazoles.[19–21] On the other hand, an analogous method for obtaining 1,5-disubstituted triazoles is less developed and generally less efficient. A common approach is the Ru(II)-catalyzed azide–alkyne cycloaddition (RuAAC).[22,23]

The literature provides few examples of azide–alkyne cycloaddition (AAC) reactions mediated by molecular containers.[24–26] These reactions were regioselective, producing the 1,4-disubstituted triazole isomer, and experienced significant accelerations. The acceleration factors, quantified as effective molarity (EM = k_{intra}/k_{bulk}), were in the range of 10–10^4 M.[27]

We recently described the acceleration of AAC reactions, Huisgen reactions, included in the cavity of the self-assembled [4 + 2] octa-imine bis-calix[4]pyrrole cage **1**.[28] The AAC reactions involved 4-azido(alkyl) pyridine-*N*-oxide derivatives, **2b–c**, and the 4-ethynyl pyridine-*N*-oxide, **3** (Fig. 1). The functionalization of the cavity of cage **1** with eight inwardly directed NH polar groups constitutes the most significant difference with respect to other molecular flasks used in mediating the AAC reaction. This particularity allowed using highly directional interactions, *i.e.*, hydrogen bonds, to drive the inclusion of the substrates and suitably orient their reacting groups in a productive geometry. In turn, it produced acceleration factors, quantified as EM, larger than 10^3 M. These represent the largest accelerations reported to date for bimolecular reactions included in a molecular container, in which the direct detection of the ternary Michaelis complex simplifies the analysis of the kinetic data. As in other examples, the mediated AAC reaction was regioselective, producing exclusively the 1,4-disubstituted isomer (*i.e.* **5b** and **5c**).

We undertook this work because the AAC reaction between **2a** and **3** was not noticeably accelerated when it was included in **1** (Fig. 1).[28] In contrast, and as mentioned above, that of **2b** with **3** was indeed significantly accelerated. The only difference between **2a** and **2b** was the incorporation of a methylene unit spacing the reacting azide group and the pyridine-*N*-oxide knob.

We became interested in evaluating the reactivity and acceleration effect caused by adding the methylene spacer unit in the alkyne substrate instead of the azide. Herein, we report our findings for analogous AAC reactions confined in cage **1** using 1-(2-propynyl)-4-pyridinone, **4**, as the alkyne substrate. Pyridinone **4** is the surrogate of the desired homologous of pyridine-*N*-oxide **3** that was synthetically elusive for us.

We use ^{1}H NMR titrations to characterize the formation of 1 : 1 and 2 : 1 homo-complexes by including **4** in cage **1**. The results of related experiments with the series of azido(alkyl) pyridine-*N*-oxides, **2a–c**, were already reported.[28] Mixing equimolar amounts of an azido-derivative, **2a–c**, with 1-(2-propynyl)-4-pyridinone **4** and cage **1** allowed the detection and characterization of the corresponding ternary hetero-complexes (Michaelis) in solution: **(2·4)⊂1**. We investigate the kinetics and regioselectivities of the AAC reactions emanating from the **(2·4)⊂1** complexes. The obtained results demonstrate acceleration of the reactions and change in regioselectivity. The cycloaddition reactions of **4** with **2b–c** mediated by cage **1** are highly regioselective for the 1,5-disubstituted triazole isomers, **8b–c** (Fig. 1). This isomer is challenging to synthesize in a good yield and regioselective manner using metal-catalyzed approaches (*e.g.* RuAAC). Our findings represent the first reported case of 1,5-regioselectivity in AAC reactions mediated by molecular containers, marking a significant and novel contribution to the field.

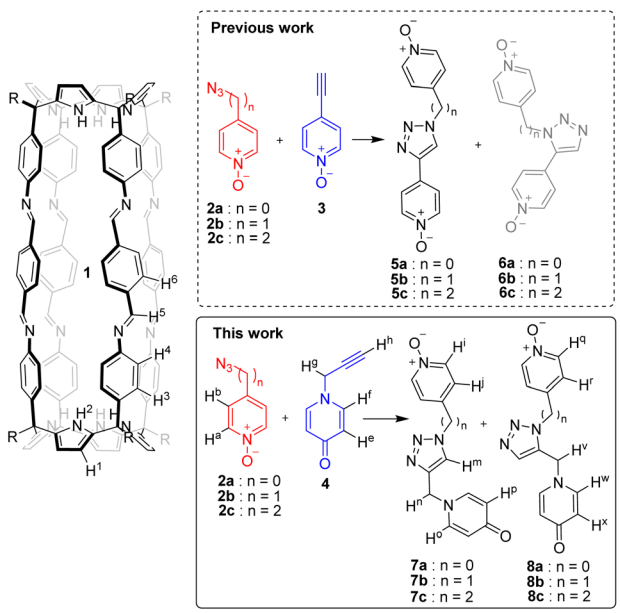

Fig. 1 Molecular structure of octa-imine cage **1** and scheme of the 1,3-dipolar cycloaddition reaction between azido-(**2a–2c**) and ethynyl (**3** or **4**) producing the two regioisomeric 1,4- (**5** or **7**) and 1,5- (**6** or **8**) disubstituted 1,2,3-triazoles. The corresponding proton assignments for octa-imine **1**, substrates **2**, and **4**, and products **7** and **8** are also shown.

Results and discussion

Synthesis

Octa-imine cage **1** and azido pyridine-*N*-oxide derivatives **2a–c** were prepared following reported procedures.[28,29] Notably, in this work, we isolated the octa-imine cage **1**. Following the quantitative self-assembly of the octa-imine cage **1** in solution, the solvent was removed under vacuum. The reaction crude was

dissolved in dichloromethane, and MeOH was added to precipitate pure **1** as a yellowish solid (DCM : MeOH 4 : 1).

The 1-(2-propynyl)-4-pyridinone **4** was prepared by reacting 4-hydroxypyridine with propargyl bromide in acetonitrile using potassium carbonate as a base.[30] Compound **4** was isolated as a white solid after column chromatography purification. We used neutral alumina as the stationary phase and a DCM: isopropyl alcohol (IPA), 97 : 3, solvent mixture as eluent (see ESI for details and complete spectroscopic characterization of the compounds).

1,4-disubstituted 1,2,3-triazole derivatives, **7a–c**, were synthesized *via* CuAAC reactions of the pyridine-*N*-oxides containing *para*-substituted azido(alkyl) residues, **2a–2c**, and 1-(2-propynyl)-4-pyridinone **4**. Analytical quantities of the 1,5-disubstituted counterparts, **8b–c**, were obtained after HPLC purification of the reaction crudes of the uncatalyzed thermal cycloaddition reactions performed at 343 K in DMF solution. The reaction crudes contained the two regioisomeric 1,2,3-triazoles, **7** and **8**, in a ~3 : 1 molar ratio, respectively.‡ We used an analytical BEH HILIC column and a linear solvent gradient elution of $CH_3CN : H_2O$ (98 : 2 to 60 : 40 in 15 minutes) for the isolation and purification of the two triazole isomers (see ESI for details and complete spectroscopic characterization of all compounds).

Binding studies with octa-imine cage 1

Azido pyridine-*N*-oxide derivatives, 2a–c. Previously, we described the formation of thermodynamically and kinetically highly stable 1 : 1, $(\mathbf{2}\cdot\mathbf{CD_3CN})\subset\mathbf{1}$, and 2 : 1 $(\mathbf{2})_2\subset\mathbf{1}$, inclusion complexes of octa-imine cage **1** with azido pyridine-*N*-oxide derivatives, **2a–c**.[28] In the 1 : 1 complexes, one pyridine-*N*-oxide molecule **2** was bound in one hemisphere of the octa-imine cage **1** by establishing four convergent hydrogen bonding interactions between its oxygen atom and the pyrrole NHs. A molecule of solvent (*i.e.*, CD_3CN), was included in the opposite hemisphere through hydrogen bonding interactions. In the 2 : 1 complexes, both hemispheres of cage **1** included one molecule of pyridine-*N*-oxide **2**. Their *para*-azido substituents converged in the center of the cage.

1-(2-propynyl)-4-pyridinone 4. In this study, we investigated the binding properties of the octa-imine cage **1** with 1-(2-propynyl)-4-pyridinone **4** using ^{1}H NMR spectroscopic titrations and ITC experiments in a $CDCl_3 : CD_3CN$, 9 : 1, solvent mixture. When approximately 1 equiv. of pyridinone **4** was added to a 2 mM solution of the octa-imine cage **1**, two new sets of proton signals with different intensities appeared (Fig. S25†). We assigned these signals to the inclusion complexes: 1 : 1, $(\mathbf{4}\cdot\mathbf{CD_3CN})\subset\mathbf{1}$, and 2 : 1, $(\mathbf{4})_2\subset\mathbf{1}$. We also detected weak signals corresponding to the free guest **4** and cage **1**.

Upon adding nearly to 2 equiv. of **4**, the signals of the 1 : 1 complex, $(\mathbf{4}\cdot\mathbf{CD_3CN})\subset\mathbf{1}$, disappeared, while those of the 2 : 1 complex, $(\mathbf{4})_2\subset\mathbf{1}$, increased significantly. At the same time, the signals of free **4** intensified, whereas those of free cage **1** became undetectable.

When more than 2 equiv. of **4** were added, the ^{1}H NMR spectrum of the mixture remained largely unchanged, except for the increase in the intensity of the signals corresponding to the free **4**. The presence of free **4**, even after adding 1 equiv. to the 2 mM solution of cage **1**, suggested that the overall binding constants for the 1 : 1 and the 2 : 1 complexes were lower than 10^4 M^{-1} and 10^8 M^{-2}, respectively.

To obtain more accurate binding constants, we performed ITC experiments. The computer-controlled injections of aliquots (10 μL) of a 20 mM solution of guest **4** in a $CHCl_3$: CH_3CN 9 : 1 solvent mixture into a 1 mM solution of the octa-imine cage **1**, in the same solvent mixture, placed in the calorimeter cell produced a gradual release of heat. The normalized areas of the integrated heat peaks produced a single sigmoidal binding isotherm, with inflection point centered close to a [**4**]/[**1**] molar ratio of 2 and not starting with a flat line (Fig. S52†). We fit the calorimetric data to the "two sets of sites" theoretical binding model implemented in the Microcal analysis software.[31] The fit returned the macroscopic stepwise binding constants as $K[(\mathbf{CH_3CN})_2\subset\mathbf{1} + \mathbf{4} \rightleftharpoons (\mathbf{CH_3CN}\cdot\mathbf{4})\subset\mathbf{1}] = (4 \pm 1) \times 10^3$ M^{-1} and $K[(\mathbf{CH_3CN}\cdot\mathbf{4})\subset\mathbf{1} + \mathbf{4} \rightleftharpoons (\mathbf{4})_2\subset\mathbf{1}] = (1 \pm 0.6) \times 10^4$ M^{-1}. The calculated values agreed with our estimates derived from the ^{1}H NMR titration experiment.

Study of the co-inclusion of 4-azido(alkyl) pyridine-*N*-oxides 2a–c with 1-(2-propynyl)-4-pyridinone 4

Next, we investigated the co-inclusion of *para*-azido-substituted pyridine-*N*-oxide derivatives **2** with 1-(2-propynyl)-4-pyridinone **4** in the octa-imine cage **1**. An equimolar solution of the octa-imine cage **1** with guests **2a** and **4** in $CDCl_3 : CD_3CN$, 9 : 1 solvent mixture, produced immediately after its preparation a ^{1}H NMR spectrum displaying four sets of proton signals for cage **1** (Fig. 2d). We assigned these signals as follows: three sets corresponded to the 1 : 1 complex $(\mathbf{2a}\cdot\mathbf{CD_3CN})\subset\mathbf{1}$ and the 2 : 1 homo-complexes $(\mathbf{2a})_2\subset\mathbf{1}$ and $(\mathbf{4})_2\subset\mathbf{1}$. We attributed the fourth set of signals to the ternary-hetero complex $(\mathbf{2a}\cdot\mathbf{4})\subset\mathbf{1}$. Additionally, we detected residual signals from the aromatic protons, H^e and H^f, of free **4** (Fig. 2d).

From the integral values of selected proton signals, we estimated the equilibrium concentration of the $(\mathbf{2a}\cdot\mathbf{4})\subset\mathbf{1}$ complex to be approximately 0.4 mM (Fig. S25†). Similar experiments with the azido(alkyl) pyridine-*N*-oxides **2b** and **2c** and 1-(2-propynyl)-4-pyridinone **4** yielded comparable concentrations (*ca.* 0.4 mM) for the corresponding ternary hetero-complexes $(\mathbf{2b}\cdot\mathbf{4})\subset\mathbf{1}$ and $(\mathbf{2c}\cdot\mathbf{4})\subset\mathbf{1}$ at equilibrium (Fig. S33 and S44†).

To further analyze the disproportionation equilibria ($(\mathbf{2})_2\subset\mathbf{1} + (\mathbf{4})_2\subset\mathbf{1} \rightleftharpoons 2\,(\mathbf{2}\cdot\mathbf{4})\subset\mathbf{1}$), we simulated the theoretical speciation using HySS2009 software.[32] The stability constants for the 1 : 1 and 2 : 1 homo-complexes of cage **1** with **2b** and **4** were fixed based on the values determined in separate titration experiments.[28] We then manually fit the overall stability constant, β, for the formation of the hetero-ternary complex $(\mathbf{CD_3CN})_2\subset\mathbf{1} + \mathbf{2} + \mathbf{4} \rightleftharpoons (\mathbf{2}\cdot\mathbf{4})\subset\mathbf{1}$, until the experimental and theoretical simulated concentrations of all the species aligned. From this analysis, we concluded that the stability constants of the three hetero-ternary complexes $(\mathbf{2a}\cdot\mathbf{4})\subset\mathbf{1}$, $(\mathbf{2b}\cdot\mathbf{4})\subset\mathbf{1}$, and $(\mathbf{2c}\cdot\mathbf{4})\subset\mathbf{1}$, were similar, falling within the range of 8.0×10^7 – 1.3×10^8 M^{-2} (Table 1). Further details on the comparisons between

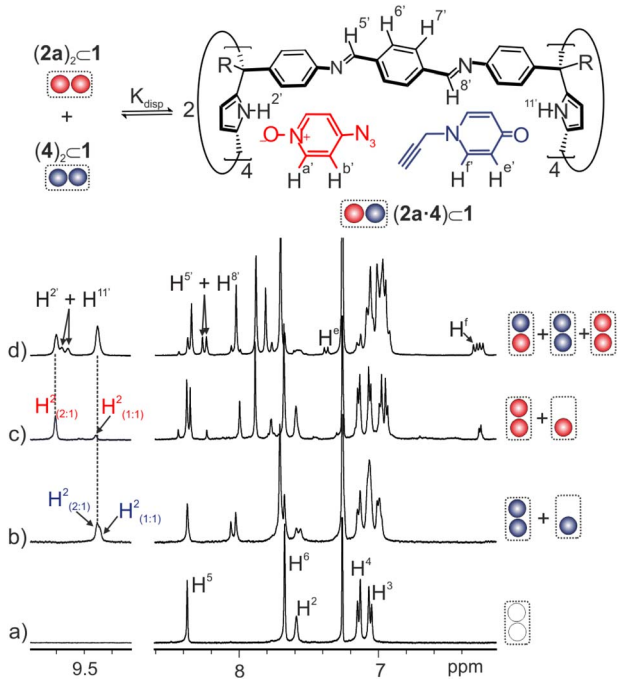

Fig. 2 (Top) disproportionation equilibrium of homo-complexes producing the ternary hetero-complex with the assignment of proton signals. (Bottom) selected regions of the ^{1}H NMR spectra (400 MHz, 298 K, $CDCl_3$: CD_3CN 9 : 1 solvent mixture) of (a) octa-imine cage **1**; (b) equimolar mixture of cage **1** with 1-(2-propynyl)-4-pyridone **4**; (c) equimolar mixture of cage **1** with 4-azido pyridine-*N*-oxide **2a**; (d) equimolar mixture of **1**, **4** and **2a** immediately after its preparation. Proton assignments in blue and red correspond to the 1 : 1 and 2 : 1 homomeric complexes of 1-(2-propynyl)-4-pyridinone **4** and 4-azido pyridine-*N*-oxide **2a**, respectively. Primed black protons correspond to the 2 : 1 heteromeric complex **(2a·4)⊂1**.

Table 1 Overall binding constants determined for the homo- and hetero-ternary complexes of octa-imine cage **1** with pyridine-*N*-oxide **2** and 1-(2-propynyl)-4-pyridinone **4**

Homo-complex	$\beta_{2:1}$ (M^{-2})	Hetero-complex	$\beta_{2:1}$ (M^{-2})
(2a)$_2$⊂1	$6.2(\pm1.2) \times 10^8$	**(2a·4)⊂1**	$8.0(\pm1.6) \times 10^7$
(2b)$_2$⊂1	$1.6(\pm0.3) \times 10^9$	**(2b·4)⊂1**	$1.3(\pm0.3) \times 10^8$
(2c)$_2$⊂1	$4.0(\pm0.8) \times 10^9$	**(2c·4)⊂1**	$1.3(\pm0.3) \times 10^8$
(4)$_2$⊂1	$4.0(\pm0.8) \times 10^7$		

experimental and theoretical speciation at equilibrium are provided in the ESI (Fig. S27, S30, S34, S37, S44, and S47).†

Using the determined β constants, the formula of the disproportionation equilibrium, $K_{dispro} = [(\mathbf{2\cdot4})\subset\mathbf{1}]^2/([(\mathbf{2})_2\subset\mathbf{1}] \times [(\mathbf{4})_2\subset\mathbf{1}]) = [\beta(\mathbf{2\cdot4})\subset\mathbf{1}]^2/([\beta(\mathbf{2})_2\subset\mathbf{1}] \times [\beta(\mathbf{4})_2\subset\mathbf{1}])$, and neglecting the presence of other equilibria in solution, we calculated an average value of K_{dispro} to be *ca.* 0.3. This value is significantly lower than the statistical estimate ($K_{dispro} = 4$) assuming isoenergetic 2 : 1 complexes. This difference derives mainly from a reduction in the stability of hetero-complexes **(2·4)⊂1** compared to those of their 2 : 1 homo-analogs of the azido-derivatives **2**. The stability reduction is likely due to steric clashes or/and repulsive dipole–dipole interactions between the two reacting groups in the hetero-complexes. This explanation also applies to the 2 : 1 complex of the 1-(2-propynyl)-4-pyridinone, **(4)$_2$⊂1**, suggesting that the termolecular complexes involving **4** are generally less stable.

Monitoring the 1,3-dipolar cycloaddition reaction of 2a with 4 included in 1

We previously reported that the AAC reaction between **2b** and **3** confined in cage **1** exhibited an exceptional acceleration factor (EM ~10^3 M) and resulted in the exclusive formation of the 1,4-triazole isomer, **5b** (Fig. 3).[28] Given the strong structural similarity between the energy-minimized conformations of the 1,4-triazole isomers **5b** and **7a** included in **1** (Fig. 3b), we hypothesized that the analogous AAC reaction of 4-azido pyridine-*N*-oxide **2a** and 1-(2-propynyl)-4-pyridone **4**, when included in cage **1** (Fig. 3c), would be selective for the 1,4-triazole isomer, **7a**, with a comparable acceleration factor.

We used ^{1}H NMR spectroscopy to monitor the evolution of a nearly equimolar (2 mM) solution mixture of **2a**, **4**, and octa-imine cage **1**. The ^{1}H NMR spectrum acquired approximately 5 min after preparing the solution, showed the expected proton signals and distribution of homo-complexes and hetero-ternary complex: **(2a·CD$_3$CN)⊂1**, **(2a)$_2$⊂1**, **(4)$_2$⊂1** and **(2a·4)⊂1**, respectively (*vide supra* and Fig. 2d). After 6 h, the ^{1}H NMR spectrum of the mixture revealed the emergence of a new set of signals for the protons of cage **1** (Fig. S27b†). Specifically, we detected two new broad signals resonating at δ = 8.8 and 8.9 ppm. We attributed these signals to the hydrogen-bonded pyrrole NHs of **1** in a new inclusion complex. The intensity of these NH signals increased over time, while the signals corresponding to the homo- and hetero-ternary complexes diminished. We concluded that the structure of the new inclusion complex should correspond to the **7a⊂1** complex, that is, the inclusion complex of the 1,4-disubstituted triazole isomer resulting from the AAC of **2a** with **4** inside cage **1**.

To further support our hypothesis, we performed a solid–liquid extraction of **7a** using a mM solution of **1**. The ^{1}H NMR

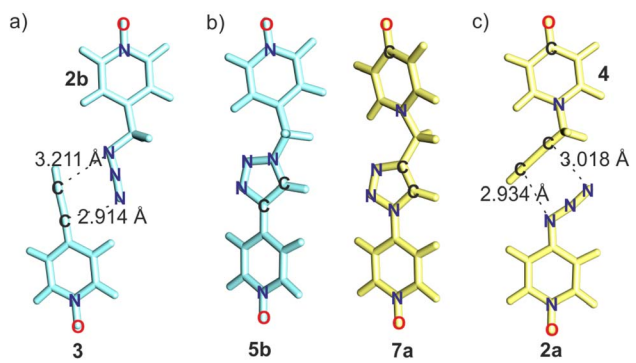

Fig. 3 (a) Arrangement of the reacting substrates in the energy-minimized structures of: (a) the **(2b·3)⊂1** ternary hetero-complex and (c) the **(2a·4)⊂1** ternary hetero-complex. The N_{azide}–$C_{acetylide}$ distances are shown. (b) Energy-minimized structures of the 1,4-triazole isomers **5b** (light-blue) and **7a** (light-yellow) in the complexes **5b⊂1** and **7a⊂1**. For clarity the structure of cage **1** is not shown in the figures.

spectrum of the filtered solution was diagnostic of the quantitative formation of the **7a**⊂**1** complex. The spectrum totally matched the proton signals of the major species detected after monitoring the reaction of **2a** with **4** in the presence of cage **1** for 16 days (Fig. S27e†). Notably, after 16 days and in the absence of **1**, a control reaction of **2a** with **4** at 2 mM concentration produced a ^{1}H NMR spectrum that only displayed the proton signals of the reactants, with no indication of the presence of signals for the two triazole isomeric products.

Taken together, these results demonstrated that the AAC reaction of **2a** with **4** was significantly accelerated in the presence of octa-imine cage **1**. Moreover, the reaction was regioselective, forming the 1,4-triazole isomer **7a**. The regioselective outcome aligned perfectly with our hypothesis, which was based on a related study's exclusive formation of the **5b**⊂**1** complex.[28] The 1,2,3-triazole spacers of **7a** and **5b** only differ in the position of the methylene unit: 4 –C for **7a** and 1 –N for **5b** (Fig. 3b).

To assess the acceleration factor of the reaction of **2a** with **4** exerted by confinement in cage **1**, we monitored the changes in the concentration of the **7a**⊂**1** complex over time by integrating selected proton signals. We fitted the kinetic data to a theoretical kinetic model accounting for six binding equilibria involving three reactants (**1**, **2a**, and **4**) alongside the irreversible cycloaddition reaction occurring within cage **1** (Fig. S29 and S58†). The equilibria produced five species: the 1 : 1 and 2 : 1 homo-complexes, as well as the hetero-complex with **1** (Fig. 4). We considered the contribution of the uncatalyzed reaction (*i.e.*, bulk reaction) to be negligible (*vide infra*), and therefore the model does not include the irreversible background thermal cycloaddition reaction. The kinetic model does not account for the dissociation of the cycloaddition product complex **7a**⊂**1** owing to its large thermodynamic stability ($K_{\mathbf{7a}\subset\mathbf{1}} > 10^6$ M^{-1}, see ESI†).

Using this kinetic analysis, the best fit of the data to the theoretical kinetic model yielded an optimized rate constant for the AAC reaction of **2a** with **4** inside cage **1** $k_{(\mathbf{7a}\text{–intra})} = (4.4 \pm 0.8) \times 10^{-6}$ s^{-1}. Separately, we determined the rate constant of the reaction producing **7a** in the bulk solution to be $k_{(\mathbf{7a}\text{–bulk})} = 6.1 \times 10^{-8}$ M^{-1} s^{-1}. From these values, we quantified the acceleration factor induced by including the AAC reaction of **2a** with **4** in cage **1** as EM = $k_{(\mathbf{7a}\text{–intra})}/k_{(\mathbf{7a}\text{–bulk})} = 7 \times 10^1$ M The measured EM is two orders of magnitude lower than the EM > 10^3 M reported for the analogous reaction of the 4-azido(methyl) pyridine-*N*-oxide **2b** with 4-ethynyl pyridine-*N*-oxide **3** included in cage **1** and exclusively producing **5b**.[28]

In summary, replacing the azide–alkyne Huisgen-pair **2b**–**3** with its structural analog **2a**–**4** did not alter the 1,4-regioselectivity of the reactions within the octa-imine cage **1**. However, it significantly impacted the reaction's acceleration factor. The TS occurring in the **(2b·3)**⊂**1** is favored by 1.6 kcal mol^{-1} over the **(2a·4)**⊂**1**. However, we lack evidence to determine whether this additional stabilization originates from entropic/enthalpic factors or from a contribution of both.

Monitoring the 1,3-dipolar AAC reaction of 2b with 4 included in 1

We reported acceleration factors of EM ≥ 10^3 M for the AAC reaction of the 4-ethynyl pyridine-*N*-oxide **3** with **2b** included in cage **1**. These results contrasted with the lack of acceleration for the analogous AAC reaction of **3** with **2a** within **1**. We were intrigued by the acceleration factor caused by increasing one methylene unit in the azide-reacting substrate, that is, using **2b** instead of **2a**, in the AAC reaction with **4** within **1**.

To investigate this, we prepared an equimolar mixture of **2b**, **4**, and cage **1**. The ^{1}H NMR spectrum acquired immediately after the solution's preparation displayed four sets of separate signals for the protons of cage **1**. We assigned these signals to the following cage complexes: **(CD$_3$CN·2b)**⊂**1**, **(2b)$_2$**⊂**1**, **(4)$_2$**⊂**1**, and **(2b·4)**⊂**1** (Fig. 5b). Additionally, we observed signals of reduced intensity corresponding to the protons of free **4**.

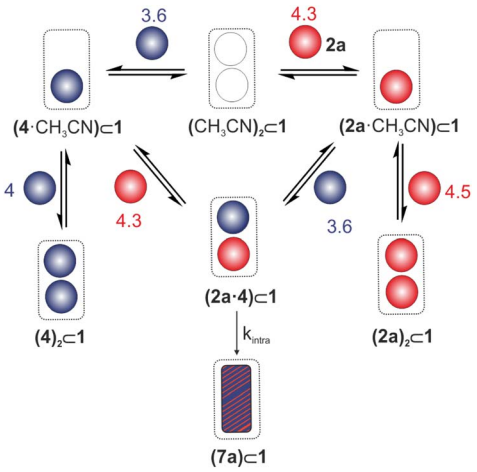

Fig. 4 Theoretical model used for the non-linear mathematical analysis of the kinetic experimental data. The log *K* value is depicted on the top of each equilibrium.

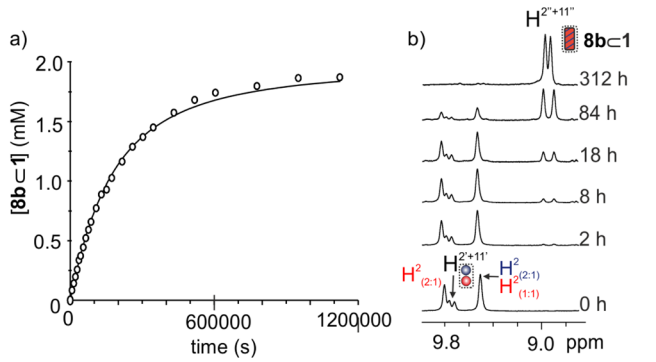

Fig. 5 (a) Changes in the concentration of **8b**⊂**1** over time determined using the integral areas of protons H$^{2'}$ and H$^{11'}$. The solid line represents the fit of the experimental kinetic data to the theoretical model using COPASI V4.25. (b) Selected region of the ^{1}H NMR spectra of the kinetic study of the formation of **8b**⊂**1** starting from a 1 : 1 : 1 mixture of **2b**, **4**, and octa-imine cage **1**. The selected region corresponds to the area in the ^{1}H NMR spectrum where the pyrrole NH protons resonate.

Using ^{1}H NMR spectroscopy, we monitored the solution mixture's evolution over a period of two weeks (Fig. 5). After 2 hours, we detected the emergence of two new signals for the NH protons of cage **1**. We attributed these signals to the complex of the cycloaddition product. After 12 days, this complex became the predominant species in the solution (Fig. 5b). We no longer detected any of the proton signals of the initially formed cage complexes. We concluded that the confined AAC cycloaddition reaction between **4** and **2b** had progressed nearly to completion within 12 days. This result represented a significant acceleration compared to the reaction of **4** with **2a** in the cavity of **1** (*vide supra*, less than 50% of conversion after 12 days, Fig. S27d†). Nevertheless, both reactions were highly regioselective. We demonstrated that the AAC reaction of **4** with **2a** confined in cage **1** selectively produced the 1,4-triazole isomer, **7a**. Similarly, we hypothesized that the confinement of **4** with **2b** in the cavity of **1** would lead to the selective formation of the 1,4-triazole isomer **7b** as the primary cycloaddition product.

We added solid **7b** to a mM solution of cage **1**. After filtration, the ^{1}H NMR spectrum of the filtered solution corresponding to the **7b**⊂**1** complex, did not match the proton signals of the major species detected after the quantitative reaction of **4** with **2b** mediated by **1**. In contrast, the proton signals of the major species of the reaction perfectly matched those of the **8b**⊂**1** complex (Fig. S34†).§ This observation indicated that, compared to previous examples of AAC reactions confined in cage **1**, the reaction of **4** with **2b** experienced a switch in regioselectivity. Notably, by enhancing the signal intensity of the ^{1}H NMR spectrum registered at the end of the AAC reaction of **4** with **2b** mediated by **1**, we could detect the presence of traces of the **7b**⊂**1** complex in the solution (<3%) (Fig. S35a†). The significant change in triazole regioisomers' ratio, **7b** : **8b**, from 75 : 25 in bulk§ to 3 : 97 in cage **1**, demonstrated the strong influence of cage **1** in controlling the regioselectivity of the included AAC reaction.

To further investigate the change in the reaction's regioselectivity, we performed density functional theory (DFT) calculations at the RI[33–35]-BP86 [33]-D3BJ[36,37] def2-TZVP[38,39] level, as implemented in Turbomole v.7.8,[40] on the energies and structures of the inclusion complexes **7b**⊂**1** and **8b**⊂**1**, and two conformers of the ternary hetero-complexes leading to their formation $(\mathbf{2b}\cdot\mathbf{4})^{1,4}\subset\mathbf{1}$ and $(\mathbf{2b}\cdot\mathbf{4})^{1,5}\subset\mathbf{1}$, respectively (Fig. 6 and 7). We also localized and optimized the transition state geometries leading to the two isomeric complexes **7b**⊂**1** and **8b**⊂**1** using DFT calculations at the RI[33–35]-BP86 [33]-def-SV(P)[38,39] level, as implemented in Turbomole v.7.0.[40] The optimized structures are in agreement with those expected for late transition states.

The results of our calculations showed that the two triazole isomers, **7b** and **8b**, are size- and shape-compatible, as well as functionally complementary to the polar cavity of the octa-imine cage **1** (Fig. 7). Additionally, the energy-minimized structures of the two conformers of the ternary complex $(\mathbf{2b}\cdot\mathbf{4})^{1,4}\subset\mathbf{1}$ and $(\mathbf{2b}\cdot\mathbf{4})^{1,5}\subset\mathbf{1}$ (Fig. 6) showed that, in both of them, the reacting groups were well positioned to achieve the TS geometry. This was particularly evident for the $(\mathbf{2b}\cdot\mathbf{4})^{1,5}\subset\mathbf{1}$ conformer, where the distances between the carbon and nitrogen atoms of the

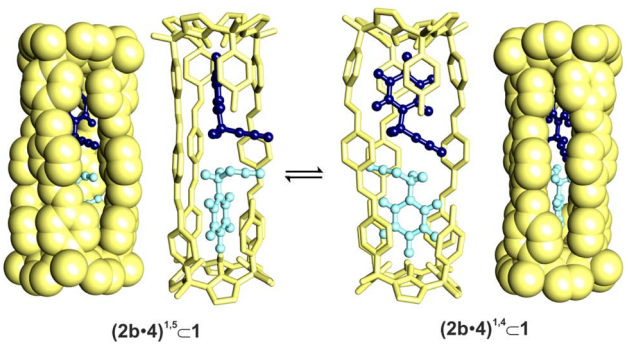

Fig. 6 Equilibrium between two different conformers of the ternary hetero-complex $(\mathbf{2b}\cdot\mathbf{4})\subset\mathbf{1}$ displaying the included reactive groups in different orientations favoring the 1,5- (left $(\mathbf{2b}\cdot\mathbf{4})^{1,5}\subset\mathbf{1}$) and the 1,4- (right $(\mathbf{2b}\cdot\mathbf{4})^{1,4}\subset\mathbf{1}$) disubstituted triazole product, respectively. Guests are shown in ball and stick representation, dark-blue for 1-(2-propynyl)-4-pyridinone **4** and light-blue for azido(methyl) pyridine-*N*-oxide **2a**. In the equilibrium, cage **1** is shown in stick representation with one of the spacer linkers deleted to assist in visualizing the geometrical arrangement of the included reactive groups. The structure of the complexes with the cage rendered as CPK model is shown aside from each ball and stick representation. This representation evidences the opening of the cage portals allowing the protrusion of some sections of the included substrates through them.

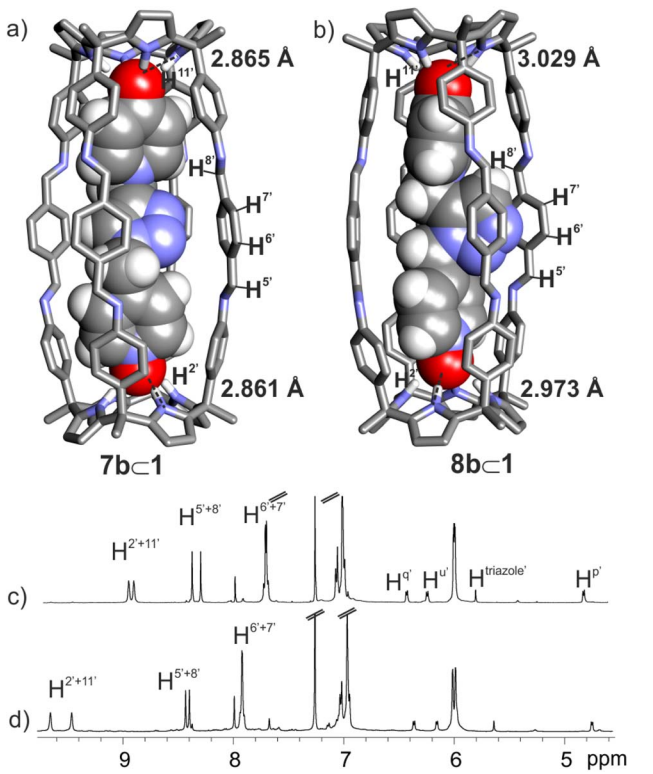

Fig. 7 (Top) energy-minimized structures (DFT) of inclusion complexes: (a) **7b**⊂**1** and (b) **8b**⊂**1**. The average hydrogen bond distance (d(H–N···O)) for each hemisphere is depicted next to the complex's structure. (Bottom) ^{1}H NMR spectra of the solutions obtained in the solid–liquid extraction experiments of the triazole isomers with a 2 mM solution of octa-imine cage **1** in a $CDCl_3$: CD_3CN 9 : 1 mixture: (c) **8b**⊂**1** and (d) **7b**⊂**1**.

dipolarophile (alkyne) and the 1,3-dipole (azide) were adequate for forming the two single bonds of the triazole in the TS (Fig. S72†). Moreover, the small computed energy difference (ΔE = 1.7 kcal mol^{-1}) favoring the **(2b·4)^{1,5}⊂1** conformer suggested that it is likely to be more prevalent in solution.

Computational studies on 1,3-dipolar cycloaddition reactions supported the idea that the TS resembled products more than starting materials.[41,42] In short, the TS of AAC reactions is product-like, mainly with respect to the bending of the 1,3-dipole.

Based on this premise, the energy difference between the products' complexes, **7b⊂1** and **8b⊂1**, should reflect more accurately the energy difference between their corresponding TSs. The calculated energy difference between these two complexes was only ∼1 kcal mol^{-1}, favoring the 1,5-triazole isomer complex, **8b⊂1**.¶ This result contrasted with the 22.4 kcal mol^{-1} energy difference calculated for the product complexes, **7a⊂1** and **8a⊂1**, which strongly favored the 1,4-triazole isomer complex, **7a⊂1**. For context, **7a** and **8a** correspond to the 1,4- and 1,5-triazole isomers, respectively, formed in the AAC reaction of **4** with **2a** (Fig. 1). While the computational results for the reaction of **4** with **2b** within **1**, did not fully account for the experimentally observed 3 : 97 ratio of **7b⊂1** to **8b⊂1** complexes (corresponding to a 2.0 kcal mol^{-1} difference), they explained the observed regioselectivity switch.‖

Filtrated solutions of separate solid–liquid extraction experiments of **7b** and **8b** with mM $CDCl_3$: CD_3CN (9 : 1) solutions of octa-imine cage **1** yielded ^{1}H NMR spectra displaying sharp and well-defined proton signals. This confirmed the good fit between the two triazole isomers, **7b**, and **8b**, and the octa-imine's **1** cavity. However, the ^{1}H NMR spectra of the two inclusion complexes, **7b⊂1** and **8b⊂1**, revealed differences in hydrogen-bonding distances. In the case of **7b⊂1**, the pyrrole NHs of the cage exhibited a complexation-induced shift (CIS = $\Delta\delta NH_{(free-bound)}$) of 2.1 ppm. In contrast, the **8b⊂1** complex showed a smaller CIS of 1.4 ppm for the analogous protons (Fig. 7c and d, respectively). These chemical shift differences suggest that the distances of the hydrogen bonding interactions established between the $N_{pyrrole}H$ of the cage and the two oxygen atoms of the different polar ends O–N/O=C of the triazole isomers are shorter in the **7b⊂1** complex than in the **8b⊂1** counterpart.

This interpretation is supported by DFT-optimized structures of the two complexes, which reveal an average hydrogen bond distance of 2.863 Å for **7b⊂1** (Fig. 7a) and 3.001 Å for **8b⊂1** (Fig. 7b). These values underscore the limited structural flexibility of cage **1**, which is unable to adapt efficiently to the different lengths of the guest isomers. Notably, in our previous studies on the binding of pyridine-*N*-oxide guests with calix[4]pyrroles, we found that optimal O···H–N hydrogen bond distances typically fall within the 2.9–3.0 Å range.[43,44] Deviations from this range – particularly the shorter distance observed in the **7b⊂1** complex – suggests a geometric mismatch between host and guest, with the guest being slightly too long to fit ideally within the rigid cavity of the host.

To determine the acceleration factor of the reaction of **4** with **2b** confined in **1**, we fit the changes in concentration of the **8b⊂1** complex over the overall reaction to the elaborated kinetic theoretical model with k_{intra}(**8b**) as single variable (Fig. S59†). The computer fit returned the optimized value of k_{intra}(**8b**) as (5.1 ± 0.4) × 10^{-5} s^{-1} (Fig. 5a and Table 2). Separately, we determined the k_{bulk}(**8b**) = 1.1 × 10^{-8} M^{-1}s^{-1} for the thermal AAC reaction of **4** with **2b**. We used the same kinetic methodology described in the previous section for the reaction between **2a** and **4**.

Using these values, we determined an EM ∼2 × 10^3 M (Table 2). This represents an acceleration two figures larger than that observed for the analogous reaction involving 4-azido pyridine-*N*-oxide **2a** instead of 4-azido(methyl) pyridine-*N*-oxide **2b**. Moreover, this EM is in the same order of magnitude as the one determined in our previous work for accelerating the reaction between **2b** and 4-ethynyl pyridine-*N*-oxide **3** (EM = 10^3 M).[28]

Taken in concert, the results of this and the previous sections highlight the strict requirements of size, shape, and function complementarity between the reacting pair of substrates and products with the container's cavity. In confined reactions, minor structural changes of the reacting substrates and products strongly influence the reaction's acceleration and regioselectivity.

To separate and compare the enthalpic and entropic components of the Gibbs energy barriers of the cycloaddition reaction between **2b** and **4**, both in the cage and in the bulk solution, we determined the reactions' rate constants (k_{bulk} and k_{intra}) at three different temperatures (298, 303, and 308 K). The activation reaction parameters, $\Delta H^{\ddagger}$ and $\Delta S^{\ddagger}$ derived from the corresponding Eyring plots (Fig. S71 and Table S5†) indicated that the observed acceleration is mainly caused by a reduction in the entropic cost associated with bringing the reactants together. Therefore, the binding of substrates in the cage primarily acts as an entropic reaction trap.

Monitoring the 1,3-dipolar cycloaddition reaction of 4 with 2c included in 1. The homologation of azido(methyl)-derivative **2b** led to its ethyl counterpart, **2c** (Fig. 1). Increasing the number of single-bond rotations that must be constrained in the reaction's TS geometry was expected to impact the reaction's

Table 2 Rate constant values for the AAC reactions in bulk (k_{bulk} ($M^{-1}s^{-1}$)) and in the cavity of octa-imine cage **1** (k_{intra} (s^{-1})). Acceleration factors, reported as effective molarities (EM, M), are also listed

Guest pair	Product	k_{bulk}[c] ($M^{-1}s^{-1}$)	k_{intra}[e] (s^{-1})	EM[f] (M)
(2b·3) [a]	1,4-**5a**	5.6 × 10^{-8}	5.0 × 10^{-5}	∼1 × 10^3
(2a·4)	1,4-**7a**	6.1 × 10^{-8}	(4.4 ± 0.8) × 10^{-6}	∼7 × 10^1
(2b·4)	1,5-**8b** [b]	2.3 × 10^{-8}	(5.1 ± 0.4) × 10^{-5}	∼2 × 10^3
(2c·4)	1,5-**8c**	n.d[d]	(4.7 ± 0.4) × 10^{-6}	[g]∼4 × 10^2

[a] See ref. 28. [b] Traces of 1,4-**7b** (<3%) were detected in the ^{1}H NMR at the end of the mediated reaction. [c] Determined by best-computer fit of the kinetic data using COPASI and a theoretical kinetic model for two competitive irreversible first-order bimolecular reactions. [d] n.d. = not determined. [e] Determined by best-computer fit of the kinetic data using COPASI and a theoretical kinetic model considering six binding equilibria, producing five different complexes and the irreversible pseudo-unimolecular reaction to produce the bound cycloaddition product. [f] EM = k_{intra}/k_{bulk} [g] We assumed that $k_{(bulk-8c)}$ can be approximated to $k_{(bulk-8b)}$.

acceleration factor negatively. However, we did not observe this effect in our previous study of the AAC reactions of **2** and **3** within cage **1**.[28] To determine whether this trend also applied to the AAC reactions of **2** and **4**, we used ^{1}H NMR spectroscopy to monitor the reaction kinetics of a nearly equimolar mixture of **4**, **2c**, and **1** in a $CDCl_3$: CD_3CN, 9 : 1, solvent mixture. The reaction also underwent a regioselectivity switch, yielding exclusively the inclusion complex of the 1,5-disubstituted 1,2,3-triazole isomer, **8c**⊂**1** (Fig. S45†).

Using the previously described kinetic analysis, we determined the acceleration factor for the AAC reaction of **4** with **2c** within **1**, yielding an EM ~4×10^2 M (Table 2). This EM value is one order of magnitude lower than that determined for the reaction of **4** with the shorter azido-derivative analog **2b** confined within the polar cavity of cage **1**. We attributed this difference to the expected entropic penalty associated with restricting an additional single-bond rotation in the TS of the reaction involving the ethyl-substituted substrate **2c**. Moreover, the additional methylene in **2c** compared to **2b** allows a greater number of low-energy conformational isomers in the ternary complex. The increased flexibility reduces the degree of preorganization. It is likely that both factors, entropic effects at the TS and decreased preorganization of the ternary complex, jointly contribute to the lower reaction rate observed for **2c** compared to **2b** in its reaction with **4** within cage **1**.

We performed DFT calculations of the two complexes, **7c**⊂**1** and **8c**⊂**1**, that are produced by including the 1,2,3-triazole isomers of the cycloaddition reaction of **4** with **2c** in cage **1**. Likewise, we computed the two conformers of the ternary complex $(\mathbf{4}\cdot\mathbf{2c})^{1,4}\subset\mathbf{1}$ and $(\mathbf{4}\cdot\mathbf{2c})^{1,5}\subset\mathbf{1}$, featuring a relative arrangement of reacting groups suitable to produce the **7c**⊂**1** and **8c**⊂**1** complexes, respectively, upon cycloaddition reaction. The results of our calculations assigned an energetic preference of approximately 8.1 kcal mol^{-1} in favor of the complex of the 1,5-disubstituted isomeric product, **8c**⊂**1** (see dataset collection of computational results available at ioChem-BD repository).[45,**,††] In contrast, the energy difference between the two conformers of the ternary complex was just 1.8 kcal mol^{-1}, favoring the $(\mathbf{4}\cdot\mathbf{2c})^{1,5}\subset\mathbf{1}$ conformer having a suitable arrangement of reacting groups to produce the 1,5-triazole isomer upon cycloaddition reaction. As mentioned earlier, the regioselectivity level of the reaction can be better explained by correlating the energy difference between the cage complexes of the cycloaddition isomeric products, **7c**⊂**1** and **8c**⊂**1**, to the energy difference of their corresponding TSs.

The reaction of **4** with **2c** produced exclusively the **8c**⊂**1** complex. The proton signals of the **7c**⊂**1** complex were not detected in the ^{1}H NMR spectrum acquired at the end of the reaction (**8c**⊂**1** : **7c**⊂**1** < 98 : 2 molar ratio). This result allowed us to estimate a minimum value of 2.3 kcal mol^{-1} for the energy difference between the TSs yielding the **7c**⊂**1** and **8c**⊂**1** complexes, in favor of the latter.

Solid–liquid extraction experiments with guest **7c** (Fig. S48†) and **8c** (Fig. S49†) using a 2 mM solution of octa-imine cage **1** revealed marked differences in binding behavior. The ^{1}H NMR spectrum of the filtered solution obtained after extraction with **8c** showed a single set of signals corresponding to the cage protons, which we attributed to the formation of the **8c**⊂**1** complex. The absence of signals from the free cage suggests that the binding is essentially quantitative, allowing us to estimate a binding constant greater than 10^4 M^{-1} for the **8c**⊂**1** complex. In contrast, the ^{1}H NMR spectrum of the filtered solution from the extraction with **7c** showed two sets of protons for the cage, corresponding to both the **7c**⊂**1** complex and free cage **1**. We also observed the proton signals of free **7c**. These observations indicated a significantly weaker interaction, with a binding constant for the **7c**⊂**1** complex below 10^4 M^{-1}.

Both experimental and theoretical studies thus confirm the preferential binding of cage **1** for the 1,5-triazole isomer **8c** over the 1,4-isomeric counterpart **7c**.

Conclusions

The reported results highlight the critical role of the container design and the complementary size, shape, and function between its cavity, and the substrates and products in accelerating and controlling the regioselectivity of the confined 1,3-dipolar cycloaddition reactions. The Huisgen cycloaddition reactions of azido pyridine-*N*-oxide **2a** with 1-(2-propynyl)-4-pyridinone **4** within the octa-imine bis-calix[4]pyrrole cage **1** experienced an acceleration quantified with EM = 70 M. This acceleration factor is two orders of magnitude lower than the one previously determined using a related substrate pair (4-azido(methyl) pyridine-*N*-oxide **2b** and 4-ethynyl pyridine-*N*-oxide **3**). The two reactions are highly regioselective for the 1,4-triazole isomer, **7a** and **5b**, respectively, which are structurally very similar. However, the confinement of the two reactions within cage **1** produced significantly different acceleration factors, 70 *vs.* > 10^3 M.

The cycloaddition reactions of 1-(2-propynyl)-4-pyridinone **4** with azido derivatives having one (**2b**), and two (**2c**), methylene units between the azido group and the pyridine-*N*-oxide ring increased their acceleration EM factors to 2000 or 400 M, respectively, when included in cage **1**. Remarkably, the two reactions experienced a regioselectivity switch toward the 1,5-disubstituted 1,2,3-triazole isomer.

Binding studies confirmed that both, the 1,4-(**8c–b**) and 1,5-triazole (**7c–b**) isomers of the reactions are included in the cavity of the octa-imine cage **1**. The results of DFT calculations assigned greater thermodynamic stability to the cage complexes with the 1,5-disubstituted isomers, **8c–b**, over the 1,4-counterparts, **7c–b**. Correlating the energy difference of the cage complexes of the cycloaddition isomeric triazole products, **7**⊂**1** and **8**⊂**1**, with those of their corresponding TSs provided a straightforward method for explaining the observed regioselectivity.

We discovered the unprecedented switching of regioselectivity, favoring the 1,5-disubstituted triazole isomer, in AAC reactions mediated by a molecular container. Our findings emphasize the importance of molecular containers in controlling both the acceleration and product selectivity of confined reactions. We expect that our work will contribute to developing molecular reactor vessels to access challenging 1,5-

disubstituted 1,2,3-triazole isomers, which are difficult to obtain in thermal or even metal-catalyzed reactions in bulk solution.

Data availability

All dataset collection of computational results of this manuscript is available in the ioChem-BD repository and can be accessed through this link: **https://doi.org/10.19061/iochem-bd-1-388**. The dataset collection includes two .mp4 files that animate the vibrational mode associated with the transition state (*i.e.*, imaginary frequency) leading to the formation of the two isomeric complexes **7b⊂1** and **8b⊂1**.

Author contributions

Conceptualization, P.·B.; methodology, Y. L.; computational studies, P. B. and G.A.; formal analysis, P.·B., G. A. and Y. L.; writing – original draft, G. A.; writing – review and editing, P.·B., G. A., and Y. L.; supervision, P. B. All authors have read and agreed to the published version of the manuscript.

Conflicts of interest

There are no conflicts to declare.

Acknowledgements

This research was funded by MICIU/AEI/10.13039/501100011033, FEDER/UE (PID2023-149233NB-I00) and MICIU/AEI/10.13039/501100011033 (Severo Ochoa Excellence Accreditations CEX2009-000925 S and CEX2024-001469 S), CERCA Programme/Generalitat de Catalunya, AGAUR (2021 SGR 00851), and the ICIQ Foundation.

Notes and references

‡ The 3 : 1 ratio of 1,2,3-triazole regioisomers, **7** : **8**, estimated for all bulk reactions, is greater than the 1.1–2.0 range commonly mentioned for Huisgen AAC reactions, unless the acetylene component is attached to an electron-withdrawing group.[46]

§ We acquired the ^{1}H NMR spectrum of the **8b⊂1** complex by performing a solid–liquid extraction of the 1,5-triazole isomer **8b** with a mM solution of cage **1**. In turn, we isolated the 1,5-triazole **8b** by purification of the crude of the thermally promoted AAC reaction of **4** with **2b**.

¶ The calculated energy between the two transition states, $\mathbf{7b^{TS}}$⊂**1** and $\mathbf{8b^{TS}}$⊂**1**, leading to the corresponding inclusion complexes, **7b⊂1** and **8b⊂1**, was 2.4 kcal mol^{-1} in favor of the latter. This result is in line with the experimentally observed ratio of products **7b⊂1** : **8b⊂1** (3 : 97; 2.0 kcal mol^{-1}) and consistent with the energy difference of their DFT-optimized structures (∼1.0 kcal mol^{-1}).

‖ We estimated $K_{\mathbf{7b\subset1}} \sim 1 \times 10^4$ M^{-1} and $K_{\mathbf{8b\subset1}} \sim 1 \times 10^5$ M^{-1} using ITC experiments. The estimated tenfold ratio of K as corresponds to an energy difference of 1.4 kcal mol^{-1}, which agrees with the results derived from the kinetic experiments (3 : 97, ∼2 kcal mol^{-1}). Additionally, the result of a competitive equimolar binding experiment between **7b** and **8b** with cage **1** extrapolated, using COPASI, to six months to reach equilibrium, yielded a **7b⊂1** : **8b⊂1** ratio of 25 : 75, or $K_{\mathbf{8b\subset1}}/K_{\mathbf{7b\subset1}} \sim 10$, supporting the greater thermodynamic stability of the **8b⊂1** complex (1,5-triazole). See ESI Fig. S56 and S57 for details.

** Dataset collection can be accessed through this link: **https://doi.org/10.19061/iochem-bd-1-388.**

†† The calculated average hydrogen bond distances in the DFT-optimized **7c⊂1** (2.742 Å) and **8b⊂1** (2.932 Å) complexes suggest that guest **8c** is a better geometric fit for the polar cavity of cage **1**.

1 J. P. Richard, Enzymatic Rate Enhancements: A Review and Perspective, *Biochemistry*, 2013, **52**, 2009–2011.
2 M. I. Page and W. P. Jencks, Entropic Contributions to Rate Accelerations in Enzymic and Intramolecular Reactions and the Chelate Effect, *Proc. Natl. Acad. Sci. U. S. A.*, 1971, **68**, 1678–1683.
3 L.-D. Syntrivanis and K. Tiefenbacher, Reactivity Inside Molecular Flasks: Acceleration Modes and Types of Selectivity Obtainable, *Angew. Chem., Int. Ed.*, 2024, **63**, e202412622.
4 M. Yoshizawa, J. K. Klosterman and M. Fujita, Functional Molecular Flasks: New Properties and Reactions within Discrete, Self-Assembled Hosts, *Angew. Chem., Int. Ed.*, 2009, **48**, 3418–3438.
5 Z. Ashbridge and J. N. H. Reek, The multifaceted roles of MnL2n cages in catalysis, *Nat. Synth.*, 2024, **3**, 1197–1207.
6 M. Morimoto, S. M. Bierschenk, K. T. Xia, R. G. Bergman, K. N. Raymond and F. D. Toste, Advances in supramolecular host-mediated reactivity, *Nat. Cat.*, 2020, **3**, 969–984.
7 K. Wang, J. H. Jordan, X.-Y. Hu and L. Wang, Supramolecular Strategies for Controlling Reactivity within Confined Nanospaces, *Angew. Chem., Int. Ed.*, 2020, **59**, 13712–13721.
8 A. B. Grommet, M. Feller and R. Klajn, Chemical reactivity under nanoconfinement, *Nat. Nanotech.*, 2020, **15**, 256–271.
9 R. Wang and Y. Yu, Site-selective reactions mediated by molecular containers, *Beilstein J. Org. Chem.*, 2022, **18**, 309–324.
10 H. Takezawa, K. Iizuka and M. Fujita, Selective Synthesis and Functionalization of an Acyclic Methylene-Bridged-Arene Trimer in a Cage, *Angew. Chem., Int. Ed.*, 2024, **63**, e202319140.
11 X.-R. Mao, Q. Wang, S.-P. Zhuo and L.-P. Xu, Reactivity and Selectivity of the Diels–Alder Reaction of Anthracene in [Pd6L4]12+ Supramolecular Cages: A Computational Study, *Inorg. Chem.*, 2023, **62**, 4330–4340.
12 J. Huang and P. Ballester, A Bimolecular Diels–Alder Reaction Mediated by Inclusion in a Polar Bis-calix[4]pyrrole Octa-Imine Cage, *J. Am. Chem. Soc.*, 2025, **147**, 13962–13972.
13 M. Yoshizawa, M. Tamura and M. Fujita, Diels-Alder in Aqueous Molecular Hosts: Unusual Regioselectivity and Efficient Catalysis, *Science*, 2006, **312**, 251–254.
14 C. Gaeta, P. La Manna, M. De Rosa, A. Soriente, C. Talotta and P. Neri, Supramolecular Catalysis with Self-Assembled Capsules and Cages: What Happens in Confined Spaces, *ChemCatChem*, 2021, **13**, 1638–1658.
15 M. Otte, Reactions in Endohedral Functionalized Cages, *Eur. J. Org Chem.*, 2023, **26**, e202300012.
16 W. Liu and J. F. Stoddart, Emergent behavior in nanoconfined molecular containers, *Chem*, 2021, **7**, 919–947.
17 N. M. Grob, R. Schibli, M. Béhé, I. E. Valverde and T. L. Mindt, 1,5-Disubstituted 1,2,3-Triazoles as Amide

Bond Isosteres Yield Novel Tumor-Targeting Minigastrin Analogs, *ACS Med. Chem. Lett.*, 2021, **12**, 585–592.
18 R. Huisgen, Kinetics and Mechanism of 1,3-Dipolar Cycloadditions, *Angew. Chem., Int. Ed.*, 1963, **2**, 633–645.
19 J. E. Hein and V. V. Fokin, Copper-catalyzed azide–alkyne cycloaddition (CuAAC) and beyond: new reactivity of copper(i) acetylides, *Chem. Soc. Rev.*, 2010, **39**, 1302–1315.
20 M. Meldal and C. W. Tornøe, Cu-Catalyzed Azide−Alkyne Cycloaddition, *Chem. Rev.*, 2008, **108**, 2952–3015.
21 C. W. Tornøe, C. Christensen and M. Meldal, Peptidotriazoles on Solid Phase: [1,2,3]-Triazoles by Regiospecific Copper(I)-Catalyzed 1,3-Dipolar Cycloadditions of Terminal Alkynes to Azides, *J. Org. Chem.*, 2002, **67**, 3057–3064.
22 L. Zhang, X. Chen, P. Xue, H. H. Y. Sun, I. D. Williams, K. B. Sharpless, V. V. Fokin and G. Jia, Ruthenium-Catalyzed Cycloaddition of Alkynes and Organic Azides, *J. Am. Chem. Soc.*, 2005, **127**, 15998–15999.
23 M. De Tullio, A. M. Borys, A. Hernán-Gómez, A. R. Kennedy and E. Hevia, Regioselective synthesis of 1,5-disubstituted 1,2,3-triazoles catalyzed by cooperative s-block bimetallics, *Chem Catal.*, 2021, **1**, 1308–1321.
24 W. L. Mock, T. A. Irra, J. P. Wepsiec and T. L. Manimaran, Cycloaddition induced by cucurbituril. A case of Pauling principle catalysis, *J. Org. Chem.*, 1983, **48**, 3619–3620.
25 W. L. Mock, T. A. Irra, J. P. Wepsiec and M. Adhya, Catalysis by cucurbituril. The significance of bound-substrate destabilization for induced triazole formation, *J. Org. Chem.*, 1989, **54**, 5302–5308.
26 J. Chen and J. Rebek, Selectivity in an Encapsulated Cycloaddition Reaction, *Org. Lett.*, 2002, **4**, 327–329.
27 R. Cacciapaglia, S. Di Stefano and L. Mandolini, Effective Molarities in Supramolecular Catalysis of Two-Substrate Reactions, *Acc. Chem. Res.*, 2004, **37**, 113–122.
28 Y. Li, C. F. M. Mirabella, G. Aragay and P. Ballester, Acceleration and Selectivity of 1,3-Dipolar Cycloaddition Reactions Included in a Polar [4 + 2] Octa-imine Bis-calix[4] pyrrole Cage, *JACS Au*, 2025, **5**, 902–912.
29 L. Adriaenssens, J. L. Acero Sánchez, X. Barril, C. K. O'Sullivan and P. Ballester, Binding of calix[4]pyrroles to pyridine N-oxides probed with surface plasmon resonance, *Chem. Sci.*, 2014, **5**, 4210–4215.
30 C. Aubert, P. Betschmann, M. J. Eichberg, V. Gandon, T. J. Heckrodt, J. Lehmann, M. Malacria, B. Masjost, E. Paredes, K. P. C. Vollhardt and G. D. Whitener, Cobalt-Mediated [2+2+2] Cycloaddition *versus* C=H and N=H Activation of Pyridones and Pyrazinones with Alkynes: An Experimental Study, *Chem. - Eur. J.*, 2007, **13**, 7443–7465.
31 *Microcal Origin Data Analysis v7.21*, Malvern Instruments Limited.
32 L. Alderighi, P. Gans, A. Ienco, D. Peters, A. Sabatini and A. Vacca, Hyperquad simulation and speciation (HySS): a utility program for the investigation of equilibria involving soluble and partially soluble species, *Coord. Chem. Rev.*, 1999, **184**, 311–318.
33 J. P. Perdew, Density-functional approximation for the correlation energy of the inhomogeneous electron gas, *Phys. Rev. B*, 1986, **33**, 8822–8824.
34 K. Eichkorn, F. Weigend, O. Treutler and R. Ahlrichs, Auxiliary basis sets for main row atoms and transition metals and their use to approximate Coulomb potentials, *Theor. Chem. Acc.*, 1997, **97**, 119–124.
35 M. Sierka, A. Hogekamp and R. Ahlrichs, Fast evaluation of the Coulomb potential for electron densities using multipole accelerated resolution of identity approximation, *J. Chem. Phys.*, 2003, **118**, 9136–9148.
36 S. Grimme, S. Ehrlich and L. Goerigk, Effect of the damping function in dispersion corrected density functional theory, *J. Comput. Chem.*, 2011, **32**, 1456–1465.
37 S. Grimme, J. Antony, S. Ehrlich and H. Krieg, A consistent and accurate *ab initio* parametrization of density functional dispersion correction (DFT-D) for the 94 elements H-Pu, *J. Chem. Phys.*, 2010, **132**, 154104–154119.
38 D. Rappoport and F. Furche, Property-optimized Gaussian basis sets for molecular response calculations, *J. Chem. Phys.*, 2010, **133**, 134105–134111.
39 A. Schäfer, H. Horn and R. Ahlrichs, Fully optimized contracted Gaussian basis sets for atoms Li to Kr, *J. Chem. Phys.*, 1992, **97**, 2571–2577.
40 TURBOMOLE Program Package For Electronic Structure 817 Calculations. **https://www.turbomole.com**.
41 H. Daver, J. N. Harvey, J. Rebek Jr and F. Himo, Quantum Chemical Modeling of Cycloaddition Reaction in a Self-Assembled Capsule, *J. Am. Chem. Soc.*, 2017, **139**, 15494–15503.
42 D. H. Ess and K. N. Houk, Theory of 1,3-Dipolar Cycloadditions: Distortion/Interaction and Frontier Molecular Orbital Models, *J. Am. Chem. Soc.*, 2008, **130**, 10187–10198.
43 A. Galan, G. Aragay and P. Ballester, A chiral "Siamese-Twin" calix[4]pyrrole tetramer, *Chem. Sci.*, 2016, **7**, 5976–5982.
44 L. Escobar, E. C. Escudero-Adán and P. Ballester, Guest Exchange Mechanisms in Mono-Metallic PdII/PtII-Cages Based on a Tetra-Pyridyl Calix[4]pyrrole Ligand, *Angew. Chem., Int. Ed.*, 2019, **58**, 16105–16109.
45 M. Álvarez-Moreno, C. de Graaf, N. López, F. Maseras, J. M. Poblet and C. Bo, Managing the computational chemistry big data problem: the ioChem-BD platform, *J. Chem. Inf. Model.*, 2015, **55**, 95–103.
46 D. Clarke, R. W. Mares and H. McNab, Preparation and pyrolysis of 1-(pyrazol-5-yl)-1,2,3-triazoles and related compounds, *J. Chem. Soc., Perkin Trans. 1*, 1997, 1799–1804.